Electronic Supplementary Material (ESI) for Nanoscale.


Electronic Supplementary Information

# Phase angle encoded upconversion luminescent nanocrystals for multiplexing applications

Haichun Liu[1,2], Muthu K. G. Jayakumar[1], Kai Huang[1], Zi Wang[1], Xiang Zheng[1], Hans Ågren[2], and Yong Zhang*,[1,3]

[1]*Department of Biomedical Engineering, Faculty of Engineering, National University of Singapore, 117583 Singapore*
[2]*Division of Theoretical Chemistry and Biology, Royal Institute of Technology, S-10691 Stockholm, Sweden*
[3]*NUS Graduate School for Integrative Sciences and Engineering, National University of Singapore, 117456 Singapore*

**Contents:**



Address correspondence to Yong Zhang, biezy@nus.edu.sg

**1. The impulse response function of two-photon upconversion dynamic system**

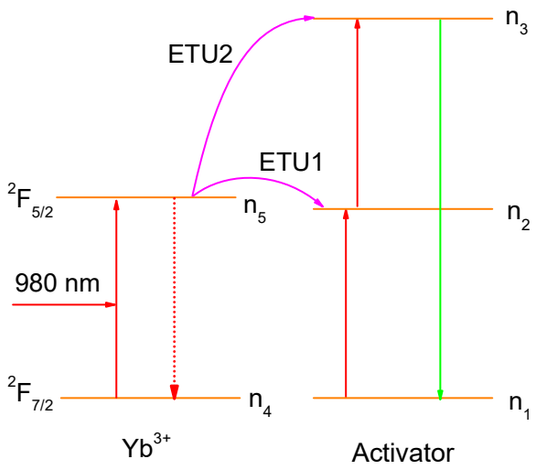


**Schematic S1** Mechanism for two-photon upconversion emission

The populations of different energy states can be described by the following rate equations:

$$\frac{dn_5}{dt} = \phi_p n_4 - \frac{n_5}{\tau_5} - W_1 n_5 n_1 - W_2 n_5 n_2 \tag{s1}$$

$$\frac{dn_2}{dt} = W_1 n_5 n_1 - W_2 n_5 n_2 - \frac{n_2}{\tau_2} \tag{s2}$$

$$\frac{dn_3}{dt} = W_2 n_5 n_2 - \frac{n_3}{\tau_3} \tag{s3}$$

where $n_i$ $(i = 1 - 5)$ denotes the population of ions at different states, and $\tau_j$ $(j = 2,3,5)$ denotes the lifetime of the excited energy levels, while $\phi_p$, $W_1$and $W_2$ represent the effective pump rate and the rate constants of energy transfer processes, labelled with ETU1 and ETU2, respectively.

The rate equations immediately following a short pulse are given by:

$$\frac{dn_5}{dt} = -\frac{n_5}{\tau_5} - W_1 n_5 n_1 - W_2 n_5 n_2 \tag{s4}$$

$$\frac{dn_2}{dt} = W_1 n_5 n_1 - W_2 n_5 n_2 - \frac{n_2}{\tau_2} \tag{s5}$$

$$\frac{dn_3}{dt} = W_2 n_5 n_2 - \frac{n_3}{\tau_3} \tag{s6}$$

In the above model, item $W_2 n_5 n_2$ in equation (s4) will be omitted as its contribution is much smaller than $\frac{n_5}{\tau_5}$ and $W_1 n_5 n_1$, yielding:

$$\frac{dn_5}{dt} = -\frac{n_5}{\tau_5'} \tag{s7}$$

where $\tau_5'$ is the effective decay lifetime of the excited state of the sensitizer ($Yb^{3+}$), given by

$$\frac{1}{\tau_5'} = \frac{1}{\tau_5} + W_1 n_1. \tag{s8}$$

Under low-power excitation conditions, upconversion is a minor kinetic perturbation. Approximating the population of level 1 ($n_1$) as a constant, thus, immediately following a short excitation pulse, the population

dynamics of energy level 5 behaves as:

$$n_5(t) = n_5(0)e^{-\frac{t}{\tau_5'}} \tag{s9}$$

Under low-power excitation conditions, the dominant deactivation channel of level 2 is via linear decay. Equation (s5) can be simplified to

$$\frac{dn_2}{dt} = W_1 n_5 n_1 - \frac{n_2}{\tau_2} \tag{s10}$$

Inserting equation (s8) into equation (s9) and rearranging the equation yields

$$\frac{dn_2}{dt} + \frac{n_2}{\tau_2} = W_1 n_1 n_5(0) e^{-\frac{t}{\tau_5'}} \tag{s11}$$

Integration over time yields

$$n_2(t) = \left( \int W_1 n_1 n_5(0) e^{-\frac{t}{\tau_5'}} e^{\int \frac{1}{\tau_2} dt} dt + C \right) e^{-\int \frac{1}{\tau_2} dt}$$

$$= \left( \int W_1 n_1 n_5(0) e^{-\left(\frac{t}{\tau_5'} - \frac{t}{\tau_2}\right)} dt + C \right) e^{-\frac{t}{\tau_2}}$$

$$= \frac{W_1 n_1 n_5(0)}{\frac{1}{\tau_2} - \frac{1}{\tau_5'}} e^{-\frac{t}{\tau_5'}} + C e^{-\frac{t}{\tau_2}}$$

where $C$ is a constant to be determined.
Assuming $n_2(0) = 0$ yields

$$C = -\frac{W_1 n_1 n_5(0)}{\frac{1}{\tau_2} - \frac{1}{\tau_5'}}, \tag{s12}$$

and thus

$$n_2(t) = \frac{W_1 n_1 n_5(0)}{\frac{1}{\tau_5'} - \frac{1}{\tau_2}} \left( e^{-\frac{t}{\tau_2}} - e^{-\frac{t}{\tau_5'}} \right) \tag{s13}$$

Inserting equations (s9) and (s13) into equation (s6) and rearranging the equation yields

$$\frac{dn_3}{dt} + \frac{n_3}{\tau_3} = \frac{W_1 W_2 n_1 n_5(0) n_5(0)}{\frac{1}{\tau_5'} - \frac{1}{\tau_2}} \left( e^{-\frac{t}{\tau_2}} - e^{-\frac{t}{\tau_5'}} \right) e^{-\frac{t}{\tau_5'}}$$

$$= \frac{W_1 W_2 n_1 n_5(0) n_5(0)}{\frac{1}{\tau_5'} - \frac{1}{\tau_2}} \left[ e^{-t\left(\frac{1}{\tau_2} + \frac{1}{\tau_5'}\right)} - e^{-\frac{2t}{\tau_5'}} \right] \tag{s14}$$

Integration over time yields

$$n_3(t) = \left( \int \frac{W_1 W_2 n_1 n_5(0) n_5(0)}{\frac{1}{\tau_5'} - \frac{1}{\tau_2}} \left[ e^{-t\left(\frac{1}{\tau_2} + \frac{1}{\tau_5'}\right)} - e^{-\frac{2t}{\tau_5'}} \right] e^{\int \frac{1}{\tau_3} dt} dt + D \right) e^{-\int \frac{1}{\tau_3} dt}$$

$$= \left( \int \frac{W_1 W_2 n_1 n_5(0) n_5(0)}{\frac{1}{\tau_5'} - \frac{1}{\tau_2}} \left[ e^{-t\left(\frac{1}{\tau_2}+\frac{1}{\tau_5'}-\frac{1}{\tau_3}\right)} - e^{-t\left(\frac{2}{\tau_5'}-\frac{1}{\tau_3}\right)} \right] dt + D \right) e^{-\frac{t}{\tau_3}}$$

$$= -\frac{W_1 W_2 n_1 n_5(0) n_5(0)}{\left(\frac{1}{\tau_5'}-\frac{1}{\tau_2}\right)\left(\frac{1}{\tau_2}+\frac{1}{\tau_5'}-\frac{1}{\tau_3}\right)} e^{-t\left(\frac{1}{\tau_2}+\frac{1}{\tau_5'}\right)} + \frac{W_1 W_2 n_1 n_5(0) n_5(0)}{\left(\frac{1}{\tau_5'}-\frac{1}{\tau_2}\right)\left(\frac{2}{\tau_5'}-\frac{1}{\tau_3}\right)} e^{-\frac{2t}{\tau_5'}} + D e^{-\frac{t}{\tau_3}} \quad \text{(s15)}$$

where $D$ is a constant to be determined.

Assuming $n_2(0) = 0$ yields

$$D = \frac{W_1 W_2 n_1 n_5(0) n_5(0)}{\left(\frac{1}{\tau_5'}-\frac{1}{\tau_2}\right)} \left[ \frac{1}{\left(\frac{1}{\tau_2}+\frac{1}{\tau_5'}-\frac{1}{\tau_3}\right)} - \frac{1}{\left(\frac{2}{\tau_5'}-\frac{1}{\tau_3}\right)} \right] \quad \text{(s16)}$$

and

$$n_3(t) = \frac{W_1 W_2 n_1 n_5(0) n_5(0)}{\left(\frac{1}{\tau_5'}-\frac{1}{\tau_2}\right)} \left\{ \left[ \frac{1}{\left(\frac{1}{\tau_2}+\frac{1}{\tau_5'}-\frac{1}{\tau_3}\right)} - \frac{1}{\left(\frac{2}{\tau_5'}-\frac{1}{\tau_3}\right)} \right] e^{-\frac{t}{\tau_3}} + \frac{e^{-\frac{2t}{\tau_5'}}}{\left(\frac{2}{\tau_5'}-\frac{1}{\tau_3}\right)} - \frac{e^{-t\left(\frac{1}{\tau_2}+\frac{1}{\tau_5'}\right)}}{\left(\frac{1}{\tau_2}+\frac{1}{\tau_5'}-\frac{1}{\tau_3}\right)} \right\} \quad \text{(s17)}$$

The sign of the premultipliers of different exponential terms is determined by relative values of $\tau_2$, $\tau_3$ and $\tau_5'$, which render them behave as exponential decay or rise. For $Yb^{3+}/Er^{3+}$-codoped systems, $W_1$ is typically in order of a few $10^{-16}$ $cm^3s^{-1}$ [1], $n_1$ is in order of a few $10^{20}$ $cm^{-3}$, $\tau_2$ in order of $10^{-3}$ s [1], and $\tau_3$ in order of $10^{-4}$ s [1]. Thus, the exponential terms $e^{-\frac{t}{\tau_3}}$, $e^{-\frac{2t}{\tau_5'}}$, and $e^{-t\left(\frac{1}{\tau_2}+\frac{1}{\tau_5'}\right)}$ in equation (s17) generally behaves as decay, decay and rise, respectively. Taken together, the impulse response function of the two-photon upconversion emission is characterized by exponential decay and rise behaviors, and the time constants are governed by (effective) decay lifetimes of involved energy states, including the excited state of sensitizer ($Yb^{3+}$), the intermediate state of activator and the excited state of the activator.

**2. Connection of the decay and rise time constants to the phase angle**

For simplicity and without loss of generality, the following IRF of upconversion emission is used,

$$I_\delta(t) = \exp\left(-\frac{t}{\tau_\mathrm{d}}\right) - \exp\left(-\frac{t}{\tau_\mathrm{r}}\right), \quad \text{(s18)}$$

where $\tau_{\mathrm{d(r)}}$ denotes the apparent decay (rise) time constant. The sinusoidally modulated excitation light is described by

$$I_\mathrm{exc}(t) = a + b\cos\omega t, \quad \text{(s19)}$$

where $b$ is the modulation amplitude, and $a$ is the modulation offset, corresponding to the average excitation intensity, and $\omega$ is the modulation circular frequency. The induced luminescence is forced to respond with the same frequency, but the phase shift and modulation depth will be varied. The resulting time-dependent luminescence intensity $I_\mathrm{f}(t)$ is given by the convolution of the squared excitation function with the IRF, *i.e.*,

$$I_\mathrm{f}(t) = \int_0^\infty I_\delta(t') I_\mathrm{exc}^2(t-t')dt'. \quad \text{(s20)}$$

Note the power of two comes into force due to the general quadratic dependence of two-photon upconversion emission on the excitation intensity when weak excitation condition is fulfilled [2,3].

Substitution of equations (s18) and (s19) yields

$$I_{\mathrm{f}}(t) = \int_0^{\infty} \left[\exp\left(-\frac{t'}{\tau_{\mathrm{d}}}\right) - \exp\left(-\frac{t'}{\tau_{\mathrm{b}}}\right)\right] \left[a + b\cos\left(\omega t - \omega t'\right)\right]^2 dt'$$

$$= \int_0^{\infty} \left[\exp\left(-\frac{t'}{\tau_{\mathrm{d}}}\right) - \exp\left(-\frac{t'}{\tau_{\mathrm{b}}}\right)\right] \left[a^2 + \frac{b^2}{2} + 2ab\cos\left(\omega t - \omega t'\right) + \frac{b^2}{2}\cos\left(2\omega t - 2\omega t'\right)\right] dt' \quad \text{(s21)}$$

The presence of higher frequency component, $\frac{b^2}{2}\cos\left(2\omega t - 2\omega t'\right)$, results from the nonlinear excitation intensity dependence of the upconversion emission. Its weight relative to the lower frequency component, *i.e.*, $\frac{b^2/2}{2ab} = \frac{b}{4a}$, is much less than $\frac{1}{4}$, considering the fact that the modulation amplitude $b$ is significantly smaller than the modulation offset $a$ in practical experiments. Thus, the contribution of high frequency component is ignored in the following discussion, yielding

$$I_{\mathrm{f}}(t) = \int_0^{\infty} \left[\exp\left(-\frac{t'}{\tau_{\mathrm{d}}}\right) - \exp\left(-\frac{t'}{\tau_{\mathrm{b}}}\right)\right] \left[A + B\cos\left(\omega t - \omega t'\right)\right] dt' \quad \text{(s22)}$$

where $A = a^2 + \frac{b^2}{2}$, and $B = 2ab$. These integrals can be calculated by recalling the identities

$$\cos(x - y) = \cos x \cos y + \sin x \sin y \quad \text{(s23)}$$

$$\int_0^{\infty} \exp(-kx)\sin(mx)\, dx = \frac{m}{k^2 + m^2} \quad \text{(s24)}$$

$$\int_0^{\infty} \exp(-kx)\cos(mx)\, dx = \frac{k}{k^2 + m^2} \quad \text{(s25)}$$

Using these identities yields

$$\int_0^{\infty} \exp\left(-\frac{t'}{\tau_{\mathrm{d(r)}}}\right)\cos\left(\omega t - \omega t'\right) dt' = \tau_{\mathrm{d(r)}}\left[\frac{\cos\omega t}{1+\omega^2\tau_{\mathrm{d(r)}}^2} + \frac{\omega\tau_{\mathrm{d(b)}}\sin\omega t}{1+\omega^2\tau_{\mathrm{d(r)}}^2}\right] \quad \text{(s26)}$$

Hence, the time dependent fluorescence intensity is given by

$$I_{\mathrm{f}}(t) = (\tau_{\mathrm{d}} - \tau_{\mathrm{r}})\left[A + \frac{B\sqrt{(1-\omega^2\tau_{\mathrm{d}}\tau_{\mathrm{r}})^2 + \omega^2(\tau_{\mathrm{d}}+\tau_{\mathrm{r}})^2}}{(1+\omega^2\tau_{\mathrm{d}}^2)(1+\omega^2\tau_{\mathrm{r}}^2)}\cos(\omega t - \varphi_{\mathrm{u}})\right] \quad \text{(s27)}$$

where the phase angle is given by

$$\cos\varphi_{\mathrm{u}} = \frac{1-\omega^2\tau_{\mathrm{d}}\tau_{\mathrm{r}}}{\sqrt{(1-\omega^2\tau_{\mathrm{d}}\tau_{\mathrm{r}})^2 + \omega^2(\tau_{\mathrm{d}}+\tau_{\mathrm{r}})^2}} \quad \text{(s28)}$$

Expression (s27) shows that the emission is delayed by an angle $\varphi_{\mathrm{u}}$ relative to the excitation and that the emission is demodulated by a factor $\frac{B\sqrt{(1-\omega^2\tau_{\mathrm{d}}\tau_{\mathrm{r}})^2 + \omega^2(\tau_{\mathrm{d}}+\tau_{\mathrm{r}})^2}}{A(1+\omega^2\tau_{\mathrm{d}}^2)(1+\omega^2\tau_{\mathrm{r}}^2)} / (\frac{b}{a})$ relative to the excitation.

**3. Numerical simulations of the phase angle in response to harmonic-wave excitation of the $Yb^{3+}/Er^{3+}$ codoped upconversion system**

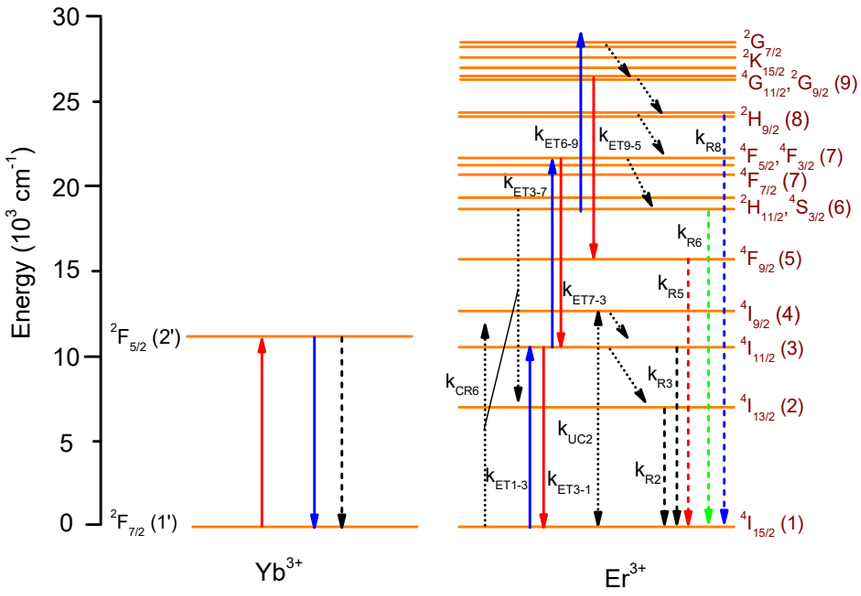


**Schematic S2** Energy level diagram illustrating the essential steps in the ETU mechanisms of $Yb^{3+}/Er^{3+}$ codoped upconversion system

The upconversion mechanism of the $Er^{3+}$ emission in $NaYF_4$:$Yb^{3+}$,$Er^{3+}$ nanocrystals is depicted in **Schematic S2**. The upconversion processes in $Yb^{3+}/Er^{3+}$ codoped system can be described by the rate equations of energy transfer [1]. According to the proposed energy transfer upconversion processes, the rate equations of each energy states are derived as follows [1]:

$Yb^{3+}$ ($^2F_{5/2}$):

$$\frac{dn_2'}{dt} = \frac{I_{ex}(t)}{hc/\lambda}\sigma n_1' - k_{Yb}n_2' - k_{ET1-3}n_1n_2' - k_{ET3-7}n_3n_2' - k_{ET5-8}n_5n_2' - k_{ET6-9}n_6n_2' + k_{ET3-1}n_3n_1' + k_{ET7-3}n_7n_1' + k_{ET9-5}n_9n_1' \quad \text{(s29)}$$

$Yb^{3+}$ ($^2F_{7/2}$):

$$\frac{dn_1'}{dt} = -\frac{dn_2'}{dt} \quad \text{(s30)}$$

$Er^{3+}$ ($^4I_{15/2}$):

$$\frac{dn_1}{dt} = k_{R2}n_2 + 0.81k_{R3}n_3 + 0.90k_{R5}n_5 + 0.70k_{R6}n_6 + 0.40k_{R8}n_8 - k_{CR6}n_6n_1 - k_{CR4}n_4n_1 + k_{UC2}n_2n_2 - k_{ET1-3}n_1n_2' + k_{ET3-1}n_3n_1' \quad \text{(s31)}$$

$Er^{3+}$ ($^4I_{13/2}$):

$$\frac{dn_2}{dt} = k_{NR3}n_3 + 0.19k_{R3}n_3 + 0.05k_{R5}n_5 + 0.25k_{R6}n_6 + 0.42k_{R8}n_8 + k_{CR6}n_6n_1 + 2k_{CR4}n_4n_1 - 2k_{UC2}n_2n_2 - k_{R2}n_2 \quad \text{(s32)}$$

$Er^{3+}$ ($^4I_{11/2}$):

$$\frac{dn_3}{dt} = k_{NR4}n_4 + k_{ET1-3}n_1n_2' + k_{ET7-3}n_7n_1' + k_{CR6}n_6n_1$$

$$+0.05k_{R5}n_5 + 0.05k_{R6}n_6 + 0.14k_{R8}n_8 - k_{ET3-1}n_3n_1^{'}$$
$$-(k_{NR3} + k_{R3})n_3 - k_{ET3-7}n_3n_2^{'} \quad \text{(s33)}$$

$Er^{3+}$ ($^4I_{9/2}$): $\frac{dn_4}{dt} = k_{UC2}n_2n_2 - k_{CR4}n_4n_1 - k_{NR4}n_4$ (s34)

$Er^{3+}$ ($^4F_{9/2}$): $\frac{dn_5}{dt} = k_{NR6}n_6 + 0.04k_{R8}n_8 - k_{ET5-8}n_5n_2^{'}$

$$+k_{ET9-5}n_9n_1^{'} - k_{R5}n_5 \quad \text{(s35)}$$

$Er^{3+}$ ($^4S_{3/2}$,$^2H_{11/2}$): $\frac{dn_6}{dt} = k_{NR7}n_7 - k_{ET6-9}n_6n_2^{'} - k_{CR6}n_6n_1 - (k_{NR6} + k_{R6})n_6$ (s36)

$Er^{3+}$ ($^4F_{7/2}$,$^4F_{5/2}$,$^4F_{3/2}$): $\frac{dn_7}{dt} = k_{NR8}n_8 + k_{ET3-7}n_3n_2^{'} - k_{ET7-3}n_7n_1^{'} - k_{NR7}n_7$ (s37)

$Er^{3+}$ ($^2H_{9/2}$): $\frac{dn_8}{dt} = k_{ET5-8}n_5n_2^{'} + k_{NR9}n_9 - (k_{NR8} + k_{R8})n_8$ (s38)

$Er^{3+}$ ($^4G_{11/2}$,$^2G_{9/2}$): $\frac{dn_9}{dt} = k_{ET6-9}n_6n_2^{'} - k_{ET9-5}n_9n_1^{'} - k_{NR9}n_9$ (s39)

$$n_{Yb} = n_1^{'} + n_2^{'} \quad \text{(s40)}$$
$$n_{Er} = n_1 + n_2 + n_3 + n_4 + n_5 + n_6 + n_7 + n_8 + n_9 \quad \text{(s41)}$$

In these equations, $I_{ex}(t)$ represents the time dependent excitation intensity; $h$ is the Planck's constant, $c$ is the speed of light, and $\lambda$ is the wavelength of the excitation light. $\sigma$ is the absorption cross-section of $Yb^{3+}$ at the excitation wavelength. $n_i$ ($i = 1-9$) denotes the population of state $i$ of $Er^{3+}$, and $n_j^{'}$ ($j = 1,2$) refers to the population of state $j$ of $Yb^{3+}$. $k_{Ri}$ and $k_{NRi}$ denote to radiative and multiphonon relaxation rate constants from state $i$. $k_{ETi-i'}$ are $Yb^{3+}$/ $Er^{3+}$ energy transfer rate constants, with $i$ and $i'$ referring to the initial and final state of $Er^{3+}$, respectively. $k_{CRi}$ is the rate constants for cross relaxation from level state $i$ of $Er^{3+}$. $k_{Yb}$ is the intrinsic rate constant for decay of the excited state of $Yb^{3+}$. $k_{UC2}$ is the rate constant for the ETU process between adjacent $Er^{3+}$ ions at state $^4I_{13/2}$, resulting in one excited ion at $^4I_{9/2}$ and the other ion in the ground state $^4I_{15/2}$. The premultipliers of the radiative rate constants, representing the emission branching ratios, were inherited from [1]. The rate equations were solved using fourth order Runga-Kutta method using Matlab® software with a step size of 640 ns. The parameter values used in the simulations were listed in **Table S1**.

**Table S1. Summary of the parameter values used in numerical simulations**

| $\sigma$ ($cm^2$) | $n_{Yb}$ ($cm^{-3}$) | $n_{Er}$ ($cm^{-3}$) | $k_{Yb}$ ($s^{-1}$) | $k_{ET1-3}$ ($cm^3/s$) | $k_{ET3-7}$ ($cm^3/s$) | $k_{ET5-8}$ ($cm^3/s$) | $k_{ET6-9}$ ($cm^3/s$) | $k_{ET3-1}$ ($cm^3/s$) |
|---|---|---|---|---|---|---|---|---|
| $1.69\times10^{-20}$ | $1.52\times10^{21}$ | $1.52\times10^{20}$ | 613 | $1.18\times10^{-15}$ | $1.54\times10^{-15}$ | $1.76\times10^{-15}$ | $6.07\times10^{-15}$ | $2\times10^{-16}$ |
| $k_{ET7-3}$ ($cm^3/s$) | $k_{ET9-5}$ ($cm^3/s$) | $k_{NR9}$ ($s^{-1}$) | $k_{NR8}$ ($s^{-1}$) | $k_{NR7}$ ($s^{-1}$) | $k_{NR6}$ ($s^{-1}$) | $k_{NR4}$ ($s^{-1}$) | $k_{NR3}$ ($s^{-1}$) | $k_{R8}$ ($s^{-1}$) |
| $2.04\times10^{-16}$ | $2.84\times10^{-16}$ | $1.76\times10^{6}$ | 43450 | $1.0\times10^{6}$ | 26 | 22120 | 61 | 2330 |
| $k_{R6}$ ($s^{-1}$) | $k_{R5}$ ($s^{-1}$) | $k_{R3}$ ($s^{-1}$) | $k_{R2}$ ($s^{-1}$) | $k_{CR6}$ ($cm^3/s$) | $k_{CR4}$ ($cm^3/s$) | $k_{UC2}$ ($cm^3/s$) | | |
| 1510 | 2039 | 73 | 110 | $2.79\times10^{-17}$ | $8.04\times10^{-19}$ | $2.31\times10^{-17}$ | | |

The excitation function was taken as

$$I_{ex}(t) = 0.5 + 0.45\cos(2\pi ft)\ [\mathrm{W/cm^2}], \quad \text{(s42)}$$

where $f$ is the modulation frequency. The time-dependent two-photon upconversion emission at 543 nm

generated from state $^4S_{3/2}$ ($Er^{3+}$), as well as the one-photon downconversion emission at around 1 μm generated from state $^4I_{11/2}$ ($Er^{3+}$), were compared with the excitation function, and the relative phase delays were extracted.

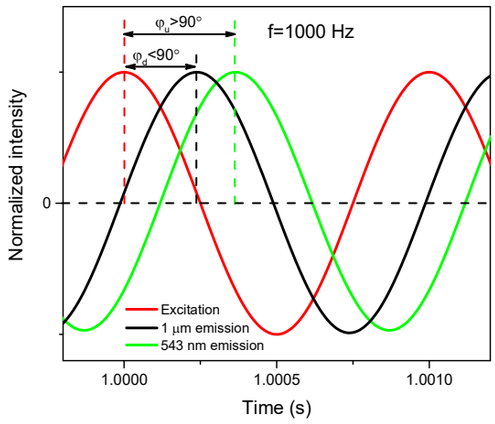


**Figure S1** Simulated harmonic response of the two-photon upconversion emission at 543 nm generated from state $^4S_{3/2}$ ($Er^{3+}$) and one-photon downconversion emission at around 1 μm generated from state $^4I_{11/2}$ ($Er^{3+}$). The modulation frequency was 1000 Hz. The phase angle of the upconversion emission is significantly larger than 90°, while that of downconversion emission remains below 90°.

## 4. Experimental details

### 4.1 Materials and reagents

$YCl_3$ (99.99%), $YbCl_3$ (99.99%), $ErCl_3$ (99.99%), $TmCl_3$ (99.99%), $LuCl_3$ (99.99%), $GdCl_3$ (99%), NaOH (97%), $NH_4F$ (98%), methanol (99.9%), oleic acid (OA, 90%), 1-octadecene (ODE, 90%), tetraethyl orthosilicate (TEOS), Igepal CO-520, ammonium hydroxide solution ($NH_4OH$, 33%), HCl (37%), were all purchased from Sigma-Aldrich. All chemicals were used as received without further purification.

### 4.2 Synthesis of $NaYF_4$:Yb,Er@$NaLuF_4$ core-shell UCNPs

$NaYF_4$:Yb,Er@$NaLuF_4$ core-shell UCNPs were synthesized through a two-step synthesis, in which the $NaYF_4$:Yb,Er core UCNPs with different concentrations of doped ions were synthesized in the first step, followed by the growth of an inert $NaLuF_4$ shell onto the as-prepared core UCNPs as seeds in the second step.

Typically, $NaYF_4$:20%Yb,2%Er core UCNPs were synthesized following a previously reported protocol with modifications [4]. $YCl_3$ (0.78 mmol), $YbCl_3$ (0.20 mmol) and $ErCl_3$ (0.02mmol) were mixed with 6 mL oleic acid and 15 mL 1-octadecene in a 100 mL flask. The solution was heated to 150 °C to form a homogenous solution and then cooled down to room temperature. A solution of 4 mmol $NH_4F$ and 2.5 mmol NaOH in 10 mL of methanol was added to the flask and stirred for 30 min. Subsequently, the solution was heated to 100 °C to remove the methanol. After methanol was evaporated, the solution was heated to 300 °C and incubated at that temperature for 1 hour under an argon atmosphere and then cooled to room temperature.

The UCNPs were precipitated with 20 mL of acetone, collected after centrifugation, then washed thrice with ethanol/water (1:1 v/v) and finally dispersed in cyclohexane for subsequent use.

The $NaLuF_4$ shell was grown onto the as-prepared core UCNPs following a previously reported protocol with modifications [5]. In a typical synthesis of $NaYF_4$:20%Yb,2%Er@$NaLuF_4$, 1 mmol $LuCl_3$ was mixed with 6 mL oleic acid and 15 mL 1-octadecene in a 100 mL flask. The solution was heated to 150 °C to form a homogenous solution and then cooled down to room temperature. A suspension of the $NaYF_4$:20%Yb,2%Er core nanocrystals dispersed in cyclohexane that obtained from the previous step was added to the flask. The solution was maintained at 110 °C to remove the cyclohexane solvent and then subsequently cooled down to room temperature. A solution of 4 mmol $NH_4F$ and 2.5 mmol NaOH in 10 mL of methanol was added to the flask and stirred for 30 min. Subsequently, the solution was heated to 100 °C to remove the methanol. After methanol was evaporated, the solution was heated to 300 °C and incubated at that temperature for 1 hour under an argon atmosphere and then cooled to room temperature. The nanocrystals were precipitated with 20 mL of acetone, collected after centrifugation, then washed thrice with ethanol/water (1:1 v/v) and finally dispersed in cyclohexane for subsequent use.

$NaYF_4$:Yb,Er@$NaLuF_4$ core-shell UCNPs with different concentration of doping ions in the core and co-doping with $Nd^{3+}$ were synthesized similarly but stoichiometrically changing the amount of lanthanide chlorides accordingly.

**4.3 Synthesis of $NaYF_4$:x%Yb@$NaYF_4$:10%Yb,2%Er@$NaLuF_4$ UCNPs**

Syntheses of $NaYF_4$:x%Yb@$NaYF_4$:10%Yb,2%Er@$NaLuF_4$ UCNPs with different concentration of $Yb^{3+}$ ions in the core were similar to the syntheses above but through a three-step synthesis and the amounts of lanthanide chlorides were changed accordingly. In order to keep similar size of the $NaYF_4$:Yb core UCNPs with varied $Yb^{3+}$ concentrations, certain amounts of $Gd^{3+}$ were co-doped to tune and maintain the core particle size.

**4.4 Synthesis of $NaYF_4$:x%Yb@$NaYF_4$:2%Yb@$NaYF_4$:2%Yb,2%Er@$NaLuF_4$ UCNPs**

Syntheses of $NaYF_4$:x%Yb@$NaYF_4$:2%Yb@$NaYF_4$:2%Yb,2%Er@$NaLuF_4$ UCNPs with different concentration of $Yb^{3+}$ ions in the core were similar to the syntheses above but through a four-step synthesis and the amounts of lanthanide chlorides were changed accordingly. In order to keep similar size of the $NaYF_4$:Yb core UCNPs with varied $Yb^{3+}$ concentrations, certain amounts of $Gd^{3+}$ were co-doped to tune and maintain the core particle size.

**4.5 Synthesis of $NaYF_4$:70%Yb@$NaYF_4$:2%Yb@$NaYF_4$:2%Yb,2%Er@$NaLuF_4$:x%Nd UCNPs**

Syntheses of $NaYF_4$:70%Yb@$NaYF_4$:2%Yb@$NaYF_4$:2%Yb,2%Er@$NaLuF_4$:x%Nd UCNPs were similar to the syntheses of $NaYF_4$:70%Yb@$NaYF_4$:2%Yb@$NaYF_4$:2%Yb,2%Er@$NaLuF_4$ UCNPs, but with certain amount of $Nd^{3+}$ ions doped into the ourtermost shell.

**4.6 Synthesis of $NaYF_4$:20%Yb,2%Er,x%Lu UCNPs**

Syntheses of $NaYF_4$:20%Yb,2%Er,x%Lu UCNPs were similar to the synthesis of $NaYF_4$:20%Yb,2%Er core nanoparticles, with addition of stoichiometric $Lu^{3+}$ ions to replace part of $Y^{3+}$.

**4.7 Synthesis of $NaYF_4$:Yb,Tm,Lu UCNPs**

Syntheses of $NaYF_4$:Yb,Tm,Lu UCNPs were similar to the synthesis of $NaYF_4$:Yb,Er core nanoparticles, with $Er^{3+}$ replaced by $Tm^{3+}$ ions and with addition of stoichiometric $Lu^{3+}$ ions to replace part of $Y^{3+}$.

**4.8 Preparation of ligand-free colloidally stable water dispersible upconversion nanocrystals**

Ligand-free colloidally stable water dispersible upconversion nanocrystals were prepared using the HCl treatment method reported previously [6]. In a typical process, 1 mL 5 mg/mL UCNP cyclohexane suspension was mixed with 1 mL 0.1 M HCl. The mixture was vortexed and then sonicated for 60 min, and most nanocrystals were transferred to the bottom aqueous layer. The top layer (cyclohexane) was discarded. The nanocrystals in the bottom layer were puried by addition of water, ethanol and aceton, followed by centrifugation (12000 rpm) for 60 min. The resulting pellets were redispersed in 1 mL water by sonication.

**4.9 Synthesis of silica-coated NaYF4:Yb,Tm,Lu upconversion nanocrystals**

$NaYF_4$:Yb,Tm,Lu upconversion nanocrystals were coated with a silica layer as follows: 1 mL of Igepal CO-520 and 18.4 mL of cyclohexane were added to 1.6 mL of 5 mg/mL UCNP cyclohexane suspension, homogenized under ultrasonication. To the solution, 160 μL of 30% $NH_4OH$ and 40 μL of TEOS was added and shaken for 48 hours. In the end, the resulting silica coated UCNPs were purified using acetone and ethanol, and finally redispersed in water.

**4.10 Encapsulation of UCNPs in polymeric beads**

UCNPs were encapsulated into beads made from PEG-DA (Polyethylene glycol diacrylate). The polymer mix was prepared using 40% (v/v) PEG-DA (molecular weight: 575), 10% (w/v) photoiniator (2-Hydroxy-4′-(2-hydroxyethoxy)-2-methylpropiophenone) and 10% (v/v) of water soluble silica-coated UCNPs. The polymer mix was spotted (3 μL/spot) on a hydrophobic PDMS film and the droplets were photo-polymerized using a UV lamp for 5 seconds per droplet. The droplets polymerized into beads, which were then transferred using a forceps onto a glass slide to make different patterns.

**4.11 Encapsulation of UCNPs in polymeric films**

UCNPs were encapsulated into polymer films of PDMS. PDMS (Dow Corning, MI) was initially mixed with a ratio of 10:1 of polymer and curing agent and mixed vigorously. Later, 100 μL of UCNP core (5 mg/mL in cyclohexane) was added to 1 mL of the polymer mixture. The mixture was then poured into a flat glass mould, divided into several different regions by thin plastic interfaces, and was degassed for 15 min and baked at 75 °C for 60 min.

**4.12 Inkjet printing of UCNPs**

Inkjet printing of UCNPs was performed using a colour inkjet printer (Canon Pixma MG3170) on standard A4 size papers. The cartridges of the printer (black and colour) were removed and the pre-filled ink was

drained completely and washed twice with water. The cartridges were then filled with different types of ligand-free UCNPs (5 mg/mL) mixed with certain amount of surfactant solution and the patterns were printed out. The colouring of the patterns was designed in CMYK colour spaces. The inkjet printer could print four different types of UCNPs simultaneously, and printing with more than four groups of UCNPs was implemented by sequentially secondary printing.

**4.13 Luminescence colour decoding**

Luminescence colour decoding was performed in a μFluor-980 small animal upconversion luminescence imaging system (Einst Technology Pte Ltd., Singapore), equipped with a continuous-wave 980 nm laser as the excitation source and different interference filters to select detection wavelength.

**5. Portable phase angle measurement system.**

Phase angle measurements in the double encryption studies and *in vivo* study were carried with a bifurcated fiber-probe based portable system. Its optical layout is illustrated in **Schematic S3**. An NIR 2 W continuous-wave laser at 980 nm (EINST Technology Pte. Ltd.), sinusoidally modulated at a specific modulation frequency by a SFG-2120 synthesized function generator (GW INSTEK), was used to provide excitation light. The laser light was guided through one branch of a bifurcated fiber cable (Avantes, 400 μm fibers, 3× SMA terminations), and illuminated the target. Generated emission light was collected by the other branch of the fiber cable, filtered by a group of filters (including 2× short pass filters at 900 nm, OD>4, and one band pass filter at the wavelength of interest, OD>4), and finally detected by an avalanche photodetector (APD130A2/M, Thorlabs). The driving signal from the function generator and the signal from the APD were coupled to a digital storage oscilloscope (Tektronix TDS2024C). The system delays, including the delay between the signal from the function generator and the excitation light at the tip of the probe, as well as time delays in the cable and circuits, were carefully corrected. The phase delay of the emission relative to the excitation was extracted by fitting the corrected profiles with cosine functions using least-square algorithm and taking the subtraction of the sought phase angles.

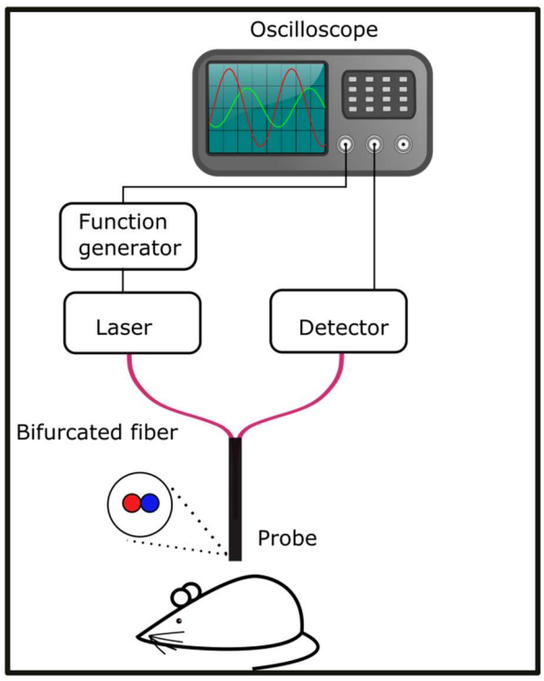


**Schematic S3** Optical layout of the bifurcated fiber-probe based harmonic response measurement system

**6. Separation of multiple groups of phase-encoded UCNPs by performing frequency-domain measurements**

When several groups of UCNPs with different phase delay features are mixed together, there is a potential to separate them (i.e., extract the concentration weight for each UCNP component) by performing frequency-domain measurements at multiple modulation frequencies followed by a multiparameter fitting procedure. This decoding process can be realized by the following two steps.

**(1) Pre-characterization of UCNP samples to extract the rise and decay time constants for each group of UCNP**.

As discussed above, the impulse response function of upconversion emission can be well approximated by

$$I_\delta(t) = \alpha_1 \exp(-t/\tau_1) - \alpha_2 \exp(-t/\tau_2),$$

where $\alpha_1 = \alpha_2$, and $\tau_1 = \tau_\mathrm{d}$, and $\tau_2 = \tau_\mathrm{b}$ according to equation (s18).

The two time constants $\tau_1$ and $\tau_2$ can be obtained by analyzing the measured frequency-domain data. The measured data are compared with values predicted from a model, and the parameters of the model are varied to yield the minimum deviations from the data. Conveniently, one may predict the frequency-dependent values of phase delay from the sine, $N_\omega$, and cosine, $D_\omega$, transforms of the impulse response function,

$$N_\omega = \frac{\int_0^\infty I_\delta(t) \sin \omega t dt}{\int_0^\infty I_\delta(t) dt}, \tag{s43}$$

$$D_\omega = \frac{\int_0^\infty I_\delta(t) \cos \omega t dt}{\int_0^\infty I_\delta(t) dt}. \tag{s44}$$

For a dual-exponential decay these transforms are

$$N_\omega \cdot J = \sum_{i=1}^{2} \frac{\alpha_i \omega \tau_i^2}{(1+\omega^2 \tau_i^2)}, \tag{s45}$$

$$D_\omega \cdot J = \sum_{i=1}^{2} \frac{\alpha_i \tau_i}{(1+\omega^2 \tau_i^2)}, \tag{s46}$$

where $J = \sum_{i=1}^{2} \alpha_i \tau_i$. The phase values can be calculated from $N_\omega$ and $D_\omega$ and are given by

$$\varphi_{c\omega} = \arctan(N_\omega / D_\omega). \tag{s47}$$

In the least-squares analysis the parameters ($\tau_1$ and $\tau_2$) are varied to yield the best fit between the measured data ($\varphi_\omega$) and the calculated values, as indicated by a minimum value for the goodness-of-fit parameters $\chi_R^2$ [7]:

$$\chi_R^2 = \frac{1}{v} \sum_\omega \left( \frac{\varphi_\omega - \varphi_{c\omega}}{\delta\varphi} \right)^2, \tag{s48}$$

where $v$ is the number of degrees of freedom, and $\delta\varphi$ is the uncertainties in the phase angle values. By performing measurements in an adequate frequency range (10 Hz – 100 kHz for upconversion emission [8]) covering the rise and decay time range (typically from a few microseconds to a few milliseconds [9]), the time constants $\tau_1$ and $\tau_2$ can be recovered.

**(2) Recover the weight of each UCNP component**

The rise and decay time constants for each UCNP component are extracted by the pre-characterization in step (1), and they will be used as knowns afterwards. When different UCNP components are mixed together, the weight for each component is the free parameters that need to be sought. In this task, the same experimental and least-squares fitting procedure as discussed in step (1) can be used.

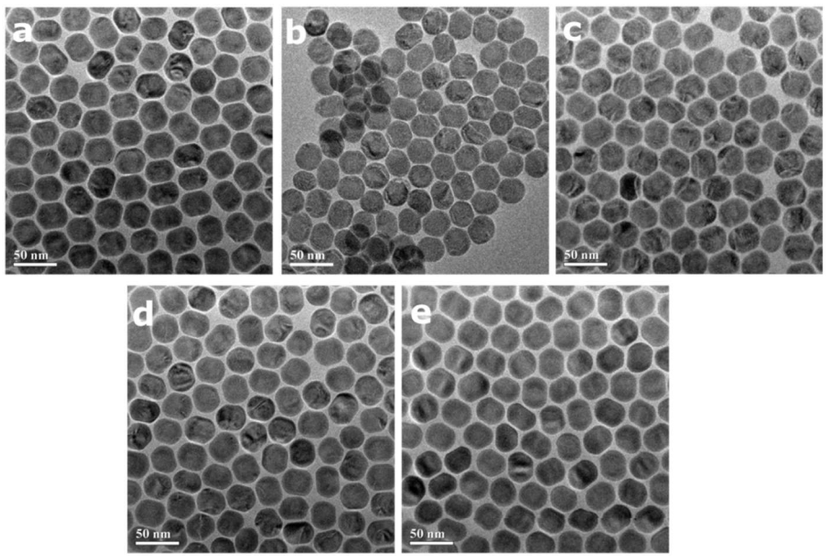


**Figure S2** Transmission electron microscopy (TEM) images of (a) $NaYF_4$:20%$Yb^{3+}$,2%$Er^{3+}$@$NaLuF_4$, (b) $NaYF_4$:60%$Yb^{3+}$,2%$Er^{3+}$@$NaLuF_4$, (c) $NaYF_4$:20%$Yb^{3+}$,8%$Er^{3+}$@$NaLuF_4$, (d) $NaYF_4$:60%$Yb^{3+}$,8%$Er^{3+}$@$NaLuF_4$, (e) $NaYF_4$:60%$Yb^{3+}$,8%$Er^{3+}$,3%$Nd^{3+}$@$NaLuF_4$ UCNPs.

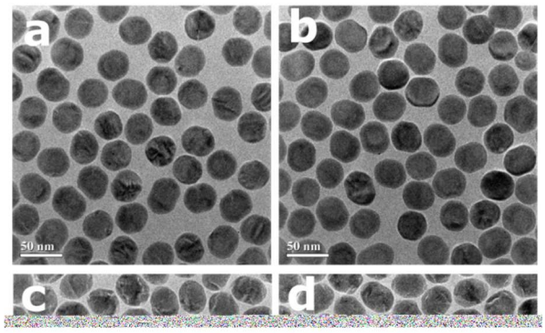


**Figure S3** TEM images of (a) $NaYF_4$:0%$Yb^{3+}$@$NaYF_4$:10%$Yb^{3+}$,2%$Er^{3+}$@$NaLuF_4$, (b) $NaYF_4$:20%$Yb^{3+}$@$NaYF_4$:10%$Yb^{3+}$,2%$Er^{3+}$@$NaLuF_4$, (c) $NaYF_4$:40%$Yb^{3+}$@$NaYF_4$:10%$Yb^{3+}$,2%$Er^{3+}$@$NaLuF_4$, (d) $NaYF_4$:70%$Yb^{3+}$@$NaYF_4$:10%$Yb^{3+}$,2%$Er^{3+}$@$NaLuF_4$ UCNPs.

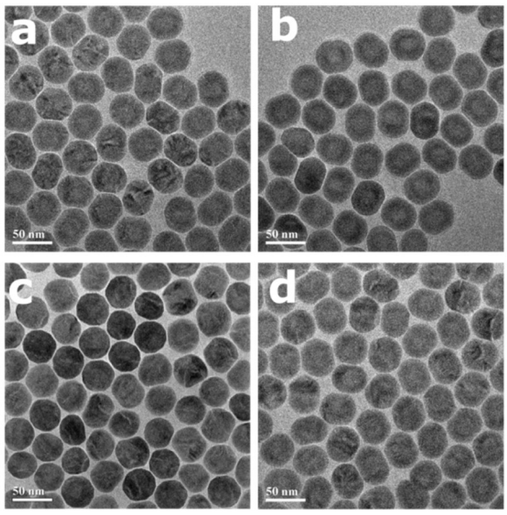


**Figure S4** TEM images of (a) $NaYF_4$:0%$Yb^{3+}$@$NaYF_4$:2%$Yb^{3+}$@$NaYF_4$:2%$Yb^{3+}$,2%$Er^{3+}$@$NaLuF_4$, (b) $NaYF_4$:15%$Yb^{3+}$@$NaYF_4$:2%$Yb^{3+}$@$NaYF_4$:2%$Yb^{3+}$,2%$Er^{3+}$@$NaLuF_4$, (c) $NaYF_4$:40%$Yb^{3+}$@$NaYF_4$:2%$Yb^{3+}$@$NaYF_4$:2%$Yb^{3+}$,2%$Er^{3+}$@$NaLuF_4$, (d) $NaYF_4$:70%$Yb^{3+}$@$NaYF_4$:2%$Yb^{3+}$@$NaYF_4$:2%$Yb^{3+}$,2%$Er^{3+}$@$NaLuF_4$ UCNPs.

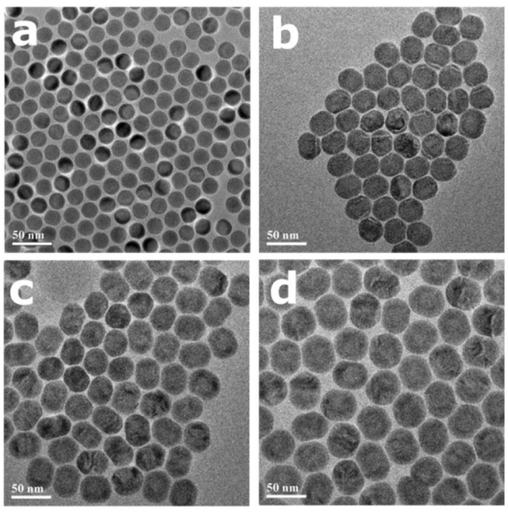


**Figure S5** TEM images of (a) $NaYF_4$:70%$Yb^{3+}$, (b) $NaYF_4$:70%$Yb^{3+}$@$NaYF_4$:2%$Yb^{3+}$, (c) $NaYF_4$:70%$Yb^{3+}$@$NaYF_4$:2%$Yb^{3+}$@$NaYF_4$:2%$Yb^{3+}$,2%$Er^{3+}$, (d) $NaYF_4$:70%$Yb^{3+}$@$NaYF_4$:2%$Yb^{3+}$@$NaYF_4$:2%$Yb^{3+}$,2%$Er^{3+}$@$NaLuF_4$ UCNPs. The average diameters of UCNPs in (a) and (b) were determined to be 21 nm and 31 nm, respectively. The thickness of the isolating/bridging $NaYF_4$:2%$Yb^{3+}$ layer was determined to ~5 nm.

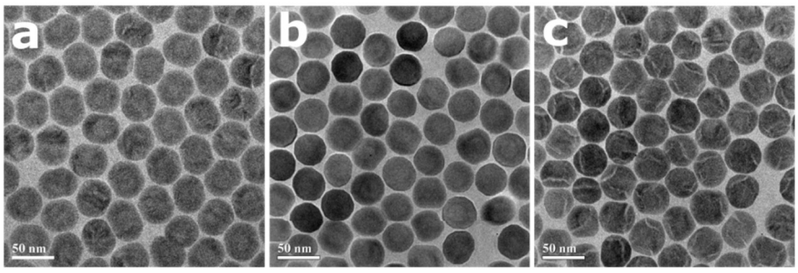


**Figure S6** TEM images of (a) $NaYF_4$:70%$Yb^{3+}$@$NaYF_4$:2%$Yb^{3+}$@$NaYF_4$:2%$Yb^{3+}$,2%$Er^{3+}$@$NaLuF_4$:0%Nd, (b) $NaYF_4$:70%$Yb^{3+}$@$NaYF_4$:2%$Yb^{3+}$@$NaYF_4$:2%$Yb^{3+}$,2%$Er^{3+}$@$NaLuF_4$:30%Nd, and (c) $NaYF_4$:70%$Yb^{3+}$@$NaYF_4$:2%$Yb^{3+}$@$NaYF_4$:2%$Yb^{3+}$,2%$Er^{3+}$@$NaLuF_4$:50%Nd UCNPs.

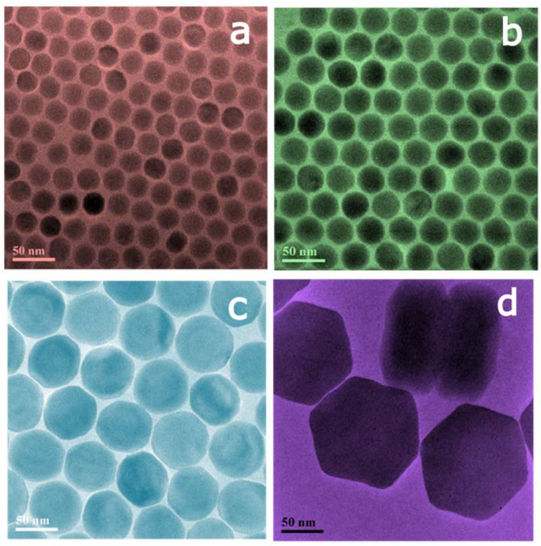


**Figure S7** TEM images of (a) $NaYF_4$:20%Yb,2%Er (G1, 25 nm), (b) $NaYF_4$:20%Yb,2%Er,20%Lu (G2, 32 nm), (c) $NaYF_4$:20%Yb,2%Er,30%Lu (G3, 68 nm), and (d) $NaYF_4$:20%Yb,2%Er,50%Lu (G4, 120 nm).

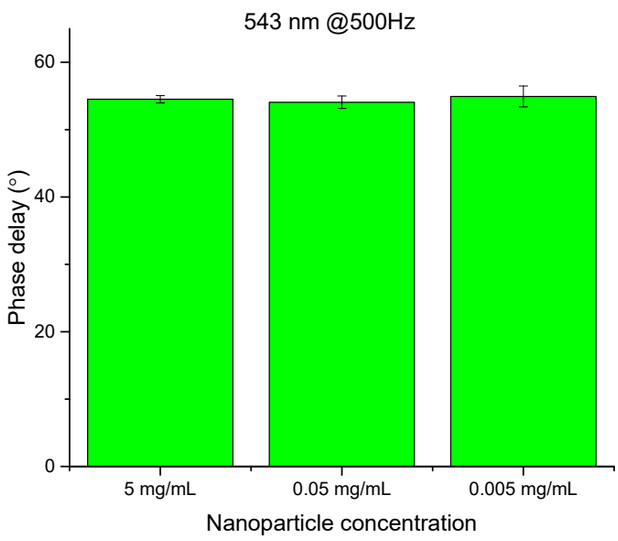


**Figure S8** The influence of nanocrystal concentration on the phase angle of $NaYF_4$:20%Yb,2%Er, 30%Lu nanocrystals, emission at 543 nm. The modulation frequency was fixed at 500 Hz, and the modulation offset and amplitude were kept as 64 W/cm$^2$ and 35 W/cm$^2$, respectively.

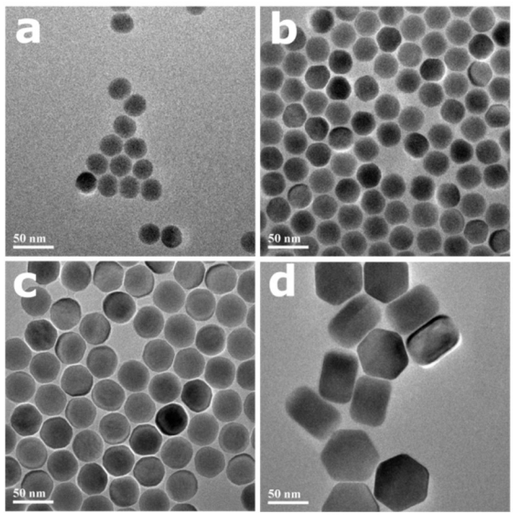


**Figure S9** TEM images of (a) $NaYF_4$:25%Yb,0.5%Tm (23 nm), (b) $NaYF_4$:25%Yb,0.5%Tm,10%Lu (31 nm), (c) $NaYF_4$:25%Yb,0.5%Tm,20%Lu (39 nm) and (d) $NaYF_4$:25%Yb,0.5%Tm,30%Lu (64 nm) UCNPs.

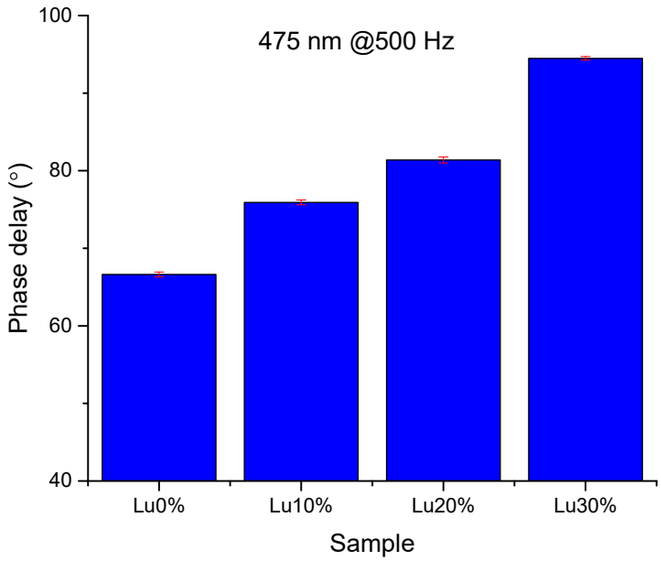


**Figure S10** The phase angles of $NaYF_4$:25%Yb,0.5%Tm (23 nm), $NaYF_4$:25%Yb,0.5%Tm,10%Lu (31 nm), $NaYF_4$:25%Yb,0.5%Tm,20%Lu (39 nm) and $NaYF_4$:25%Yb,0.5%Tm,30%Lu (64 nm) nanocrystals. The modulation frequency was fixed at 500 Hz, and the modulation offset and amplitude were kept as 64 W/cm$^2$ and 35 W/cm$^2$, respectively.

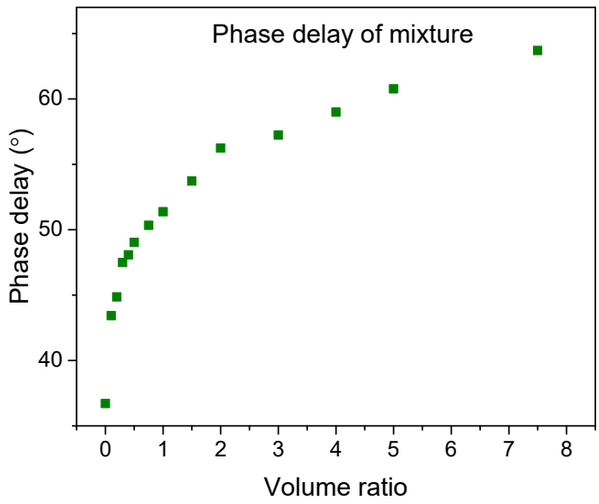


**Figure S11** The phase angles of the mixture of samples $NaYF_4$:20%Yb,2%Er (G1) and $NaYF_4$:20%Yb,2%Er,50%Lu (G4) with different volume ratio ($V_{G1}/V_{G4}$), emission at 543 nm.

**Supplementary references**


1. Anderson, R. B, Smith, S. J, May, P. S. & Berry, M. T. Revisiting the NIR-to-Visible upconversion mechanism in $\beta$-$NaYF_4$:$Yb^{3+}$,$Er^{3+}$. *J. Phys. Chem. Lett.* **5**, 36-42 (2014).
2. Suyver, J. F., Aebischer, A., García-Revilla, S., Gerner, P. & Güdel, H. U. Anomalous power dependence of sensitized upconversion luminescence. *Phys. Rev. B* **71**, 125123 (2005).
3. Liu, H. *et al*. Balancing power density based quantum yield characterization of upconverting nanoparticles for arbitrary excitation intensities. *Nanoscale* **5**, 4770-4775 (2013).
4. Li, Z., & Zhang, Y. An efficient and user-friendly method for the synthesis of hexagonal-phase $NaYF_4$:Yb,Er/Tm nanocrystals with controllable shape and upconversion fluorescence. *Nanotechnology* **19**, 345606 (2008).
5. Qian, H., & Zhang, Y. Synthesis of hexagonal-phase core-shell $NaYF_4$ nanocrystals with tunable upconversion fluorescence. *Langmuir* **24**, 12123-12125 (2008).
6. Bogdan, N., Vetrone, F., Ozin, G. A., & Capobianco, J. A. Synthesis of ligand-free colloidally stable water dispersible brightly luminescent lanthanide-doped upconverting nanoparticles. *Nano Lett*. **11**, 835-840 (2011).
7. Lakowicz, J. R., Laczko, G, & Cherek, H. Analysis of fluorescence decay kinetics from variable-frequency phase shift and modulation data. *Biophys. J.* **46**, 463-477 (1984).
8. Riuttamäki, T., Hyppänen, I., Kankare, J., & Soukka, T. Decrease in luminescence lifetime indicating nonradiative energy transfer from upconverting phosphors to fluorescent acceptors in aqueous suspensions. *J. Phys. Chem. C* **115**, 17736-17742 (2011).
9. Hyppänen, I. Frequency-domain and wide-pulse time-domain measurements of lanthanide luminescence-based resonance energy transfer. PhD thesis, University of Turku, Finland, 2012.